Journal of Modern Physics, 2023, 14, 1019-1033
https://www.scirp.org/journal/jmp
ISSN Online: 2153-120X
ISSN Print: 2153-1196

# Realization of High Efficient Ferroelectric Perovskite Nanoparticles in Biopolymer-Matrix Solar Cells under Low Lighting

**Rémi Ndioukane[1*], Fanta Baldé[1], Ndéye Coumba Yandé Fall[1], Abdoul Kadri Diallo[1], Diouma Kobor[1], Jeanne Solard[2], Laurence Motte[3]**

[1]Laboratoire de Chimie et de Physique des Matériaux (LCPM), University Assane Seck of Ziguinchor, Ziguinchor, Senegal
[2]Centrale de Proximité en Nanotechnologies de Paris Nord, Institut Universitaire de Technologie de Villetaneuse, Paris, France
[3]Laboratory for Vascular Translational Science (LVTS), University Paris 13, Paris, France
Email: *remindioukane@gmail.com

**How to cite this paper:** Ndioukane, R., Baldé, F., Fall, N.C.Y., Diallo, A.K., Kobor, D., Solard, J. and Motte, L. (2023) Realization of High Efficient Ferroelectric Perovskite Nanoparticles in Biopolymer-Matrix Solar Cells under Low Lighting. *Journal of Modern Physics*, **14**, 1019-1033.
https://doi.org/10.4236/jmp.2023.147056

**Received:** March 2, 2023
**Accepted:** June 16, 2023
**Published:** June 19, 2023



## Abstract

The idea to use ferroelectric materials (PZN-PT) came from the fact that the ferroelectric nature could facilitate electric charges accumulation on the interfaces of the solar cell. Thus, it would increase the open circuit voltage $V_{oc}$ which could reach more than 10 V. This would directly impact the efficiency which is proportional to $V_{oc}$, thus hoping to obtain solar efficiency never equaled by the halide perovskites which are less stable and less resistant in aggressive environments. In this work, the solar cells produced gave an exceptional record efficiency of 39.32% with a very high open circuit voltage ($V_{oc}$) of 3.50 V, a short-circuit current density ($J_{sc}$) of 0.118 mA/cm$^2$ and an FF of 0.72 measured in the positive polarization direction under 3825 lux (5.6 W/m$^2$) lighting. The negative polarization direction under 4781 lux (7 W/m$^2$) lightning gave a current density of 2 mA/cm$^2$, an open circuit voltage of 2.30 V and an FF of 0.35.

## Keywords

Perovskite, Nanoparticles, Thin Film, Ferrophotovoltaic, Solar Cell

## 1. Introduction

Among the various sources of renewable energy, solar photovoltaic is undoubtedly one of the best solutions for reducing the impact of fossil fuels on the environment and human health. For decades, the most widely used technology for photovoltaic conversion has been that of crystalline silicon solar cells. However, the production of crystalline silicon is very expensive because it re-

quires a lot of energy to reach crystallization temperatures which are around 1000˚C.

For years, alternatives have been proposed in order to obtain low cost and very efficient solar cells. Thus, organic cells have been studied but their efficiency unfortunately does not exceed 15% currently in the laboratory. In addition, these organic cells have a problem of time, temperature and chemical stabilities. To overcome these difficulties, organometallic halide perovskites based on tin (CsSnX) or lead (CHNHPbX) [1], have been used as an absorber layer to replace traditional organometallic complexes or organic molecules. With a conversion efficiency of 6.54% in liquid electrolyte devices and 12.3% in semiconductor devices [2], lead-based perovskite appears to be a good candidate. The efficiency of photovoltaic cells that incorporate perovskites has continued to increase dramatically, rising in record time from 12% in 2013 to more than 25% in 2022 [3].

However, the main obstacle to the development of these solar cells based on halogenated perovskites is the problem of time and temperature stability [4] and aggressive environmental problems induced by the Pb contents [5].

Currently a new type of solar cell based on ferroelectric material is emerging. Unlike conventional solar cells, in this type of solar cell, a p-n junction is not required. Interesting conversion efficiencies are beginning to be obtained with this type of cell (up to 8.1% in 2015), however the mechanisms are not yet well understood and several material and engineering challenges must be overcome. The performance of photovoltaic cells based on perovskite materials depends on several parameters, such as the cell architecture, the materials used for the active layer, the interfacial layers for electron and hole transport and the electrodes type as well as manufacturing techniques and conditions. Inorganic oxides have significant advantages. The ideal band gap for an active photovoltaic layer for the solar spectrum is around 1.3 eV. However, oxides with such values are infrequent. One of the most studied oxides to date as an active photovoltaic layer is cuprous oxide $Cu_2O$. Its bandgap is around 2.1 - 2.7 eV [6] and is therefore not ideal for the solar spectrum. The conversion efficiencies generally do not exceed 4%. Grinberg *et al.* [7] proposed, in 2013, a solar cell based on ferroelectric perovskites which made it possible, by doping $KbNO_3$ with Ba, Ni and Nb, to reduce the gap of $KbNO_3$ from 4 to 1.5 eV like that of halogenated perovskites with ferrophotovoltaic behavior. Several researchers have used different ferroelectric oxides in order to achieve high efficiency with better stability compared to halogenated perovskites. Most recently, the inorganic PZN-PT perovskite materials have been investigated for their excellent and stable properties. This ferroelectric material shows other properties such as magnetism when reduced into nanopowder form [8]. PZN-PT single crystals showed properties up to 10 times more interesting than those of the ferroelectric perovskite ceramics currently used as actuators and sensors. However, their fabrication as thin layers form is a challenge due to the presence of a pyrochlore phase around 950˚C making difficult to integrate them in electronic or solar cell devices.

From conservation efforts and cleantech to tracking of environmental con-

ditions and reductions in energy usage, every imaginable facet in the quest to reduce our carbon footprint is being explored through the Internet of Things (IoT). Thus, for indoor applications, the power supply of billions of independent electronic devices and equipment, with the advent of the IoT, is a huge energy requirement that risks compromising reduction decisions of the impact of energy consumption on the climate [9] [10] [11] [12] [13]. One of the solutions would be the use of photovoltaic cells capable of efficiently converting low intensity light in the indoor environment into megawatt to microwatt [14] [15] [16] [17] [18] class electrical power. These types of materials would be excellent candidates for powering low power equipment and appliances. In general, conventional solar cells use the standard solar spectrum with the best yields unlike these new cells which operate optimally with emission spectra from light sources at low intensities often less than 1 $mW{\cdot}cm^{-2}$ [19]. Indeed, crystalline silicon cells exhibit low power conversion efficiencies (PCEs) under indoor lighting [20] [21]. On the contrary, although some of the emerging photovoltaic cells, such as organic photovoltaic (OPV) cells and dye solar cells, are not as efficient as crystalline silicon cells under standard solar lighting, the absorption properties of the highly adjustable light of their materials make them promising candidates for interior applications [22] [23] [24] [25] [26]. Compared with dye solar cells, OPV cells have better business prospects due to the advantages of low cost, large area module through solution printing and coating techniques. In addition, they could be used as the rear face of bifacial solar cell to exploit more efficiently the low and diffuse irradiance of the sun permitting to improve its energy conversion.

Here, we present ferroelectric perovskite nanoparticles dispersed in a biopolymer thin film on ITO glass for highly efficient indoor energy harvesting. Indeed, this work proposes another way to obtain solar cells based on PZN-PT ferroelectric oxides with very high efficiency beyond that of halogenated perovskites and requiring only ferroelectric nanoparticles dispersed in biopolymer matrix thus allowing the reduction of their environmental impact. First, we successfully fabricated and demonstrated large improvement of optical and photovoltaic performances due to the presence of the PeryDA+EB layer. For this purpose, we realized Ag/np+CC/$TiO_2$/ITO, Ag/EB/np+CC/$TiO_2$/ITO, Ag/PeryDA/np+CC/$TiO_2$/ITO and Ag/PeryDA+EB/np+CC/$TiO_2$/ITO solar cells via spin coating and droplet procedures. Measurements were achieved under low lightning levels and at high lighting for comparison. PCEs obtained are respectively 0.14%, 0.010%, 9% and 39.32% at 4781 lux (7 $W/m^2$) illuminance. This is a record of power conversion of solar cells for indoor application with an open voltage ($V_{oc}$) of 3.50 V, a short-circuit current density ($J_{sc}$) of 0.118 $mA/cm^2$ and an FF of 0.72. The color coordinates represented in the CIE (Commission Internationale de l'Eclairage) chromaticity diagram (x = 0.30, y = 0.34) is close to the standard equal energy white light source (x = 0.33, y = 0.33). This result suggests that this material is very interesting for white light sources applications too.

## 2. Experimental Procedure

### 2.1. Solar Cells Fabrication

To fabricate the solar cell, the ITO used has a square resistance of 9 - 15 Ω/□, a thickness of 1200 to 1600 Å. A 30 nm $TiO_2$ charge transport layer was deposited on pre-cleaned ITO conductive glass. The mesoporous $TiO_2$ was deposited on the substrate by spin coating at a speed of 3500 rpm for 10 min with an acceleration ramp of 4 s, from a paste of titanium oxide powder diluted in acetic acid, the weight ratio of $TiO_2$ and acetic acid was 6:1, then the substrates were sintered at 450˚C for 30 min [27].

The PZN-PT single crystals were ground in a silicon carbide mortar to obtain perovskite nanopowders [8]. The biopolymer (CC) solution, which is the organic matrix in which the nanoparticles are dispersed, is obtained by organic extraction procedure. The nanoparticles are then dispersed in this CC solution and placed under magnetic stirring for 30 min to one hour. The result is a homogeneous solution containing ferroelectric oxide nanoparticles. The film of perovskite nanoparticles was deposited by spin-coating on the $TiO_2$ layer. The spin coating deposition procedure was carried out at room temperature with a rotational speed of 3500 tr/min for 5 min with an acceleration of 4s. Subsequently, the sample was placed in an oven for 30 min at 105˚C, then it was annealed at 450˚C for 30 min.

After cooling to room temperature, a charge carrier material Perylene Diimide Aniline (PeryDA) was deposited on the the perovskite layer. The droplet deposition procedure was carried out in an ambient room. The PeryDA solution was synthesized by a chemical reaction between perylene and aniline in the presence of propanoic acid at 80˚C for 20 h thus giving a reddish powder (**Figure 1**). This powder will be dissolved in distilled water or ethanol to deposit a few drops on the perovskite layer. After drying at room temperature, a natural biomolecule of (EB) was deposited on the PeryDA layer. The droplet deposition procedure was carried out in ambient conditions. The EB solution was extracted directly from a EB plant by making an incision in the bark to extract the white latex.

### 2.2. Microstructural and Morphological Characterization

The forms and dimensions of the nanoparticles were examined using transmission electron microscopy (TEM). The mean diameter of the nanoparticles is calculated using ImageJ software through Gaussian distribution of many size measurements. TEM images were taken with a Phillips CM10 using an acceleration voltage of 200 KV. Scanning electron microscopy (SEM) was used to characterize the morphologies of the different deposited layers. Surface morphology was observed by using an electron beam lithography system Pioneer Raith model in C(PN)2 (University Paris 13).

## 3. Optical Characterization

### 3.1. UV-Visible Characterization

UV-visible spectra of thin films, which were prepared by spin-coating were

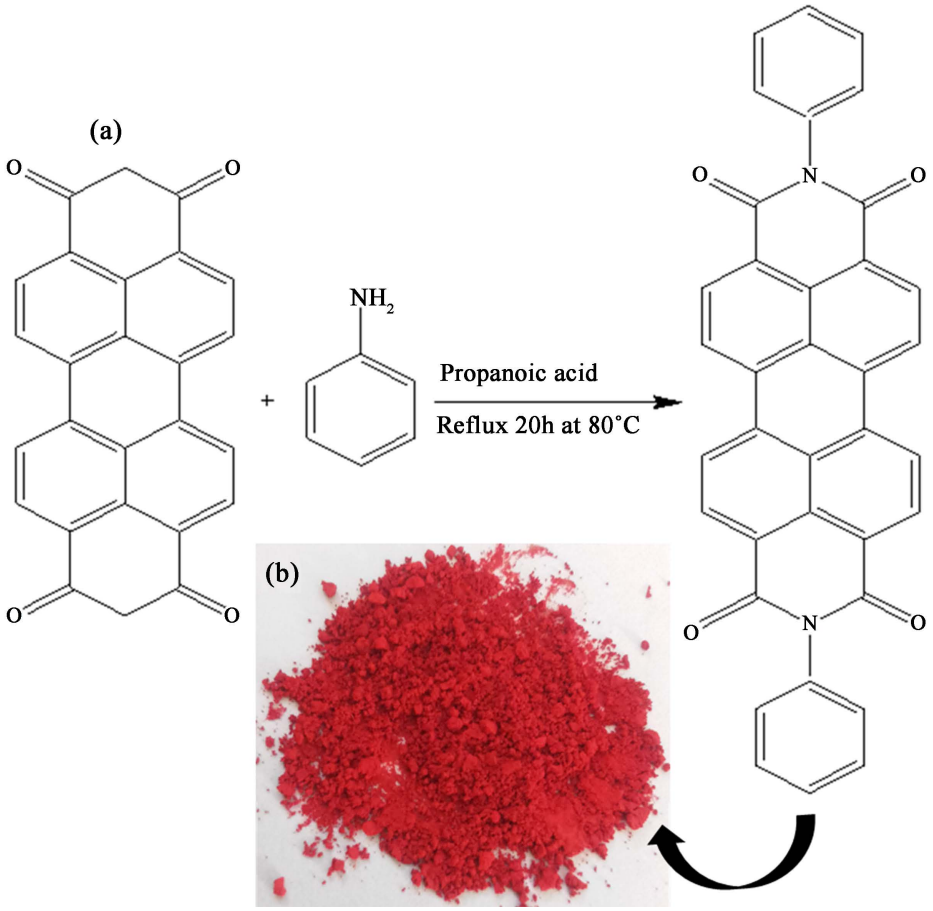


**Figure 1.** (a) Chemical reaction for the synthesis of Perylene Diimine Aniline, (b) Obtained Perylene Diimine Aniline powder.

measured out at room temperature. Optical measurement was performed using an UV Visible spectrophotometer with an integrating sphere model LAMBDA 950S in IM2NP (Marseille).

### 3.2. Photoluminescence Characterization

The excitation and emission spectra were recorded on Horiba JobinYvon Fluorolog III fluorescence spectrometer using a 450 W Xenon lamp as the excitation source. The luminescence spectra were corrected for instrumental sensitivity. CIE (Commission Internationale de l'Eclairage) emission color coordinates (x,y) were obtained using an MSU-003 colorimeter (Majantys) with PhotonProbe 1.6.0 software (Majantys).

### 3.3. Electrical Characterization

Finally, a layer of a few nm of silver paste was deposited by screen printing using a mask on a non-conductive glass and annealed at 100˚C was produced to act as an electrode for electrical measurement. The current-voltage characteristics are measured using Keithley model 2612B source meter driven by a computer under TSP Express program. The light source was a 100 W xenon lamp. The incident

power is measured using a luxmeter and desired value can be obtained by varying the distance between the sample and the incident source.

## 4. Results and Discussion

### 4.1. TEM and SEM Images

Figure 2 shows PZN-4.5PT ferroelectric perovskite nanopowder and its images from Transmission Electron Microscopy (TEM) showing their sizes and their spherical shapes with diameters varying between 30 and 100 nm. Dynamic Light Scattering DLS characteristic reveals that the average size of ferroelectric nanoparticles is around 78 nm.

Figure 3 shows SEM images revealing notable differences between the perovskite layers (Figure 3(a), Figure 3(b)). The top view of the layers gives homogeneous films with the $TiO_2$ completely covered by the perovskite nanoparticles.

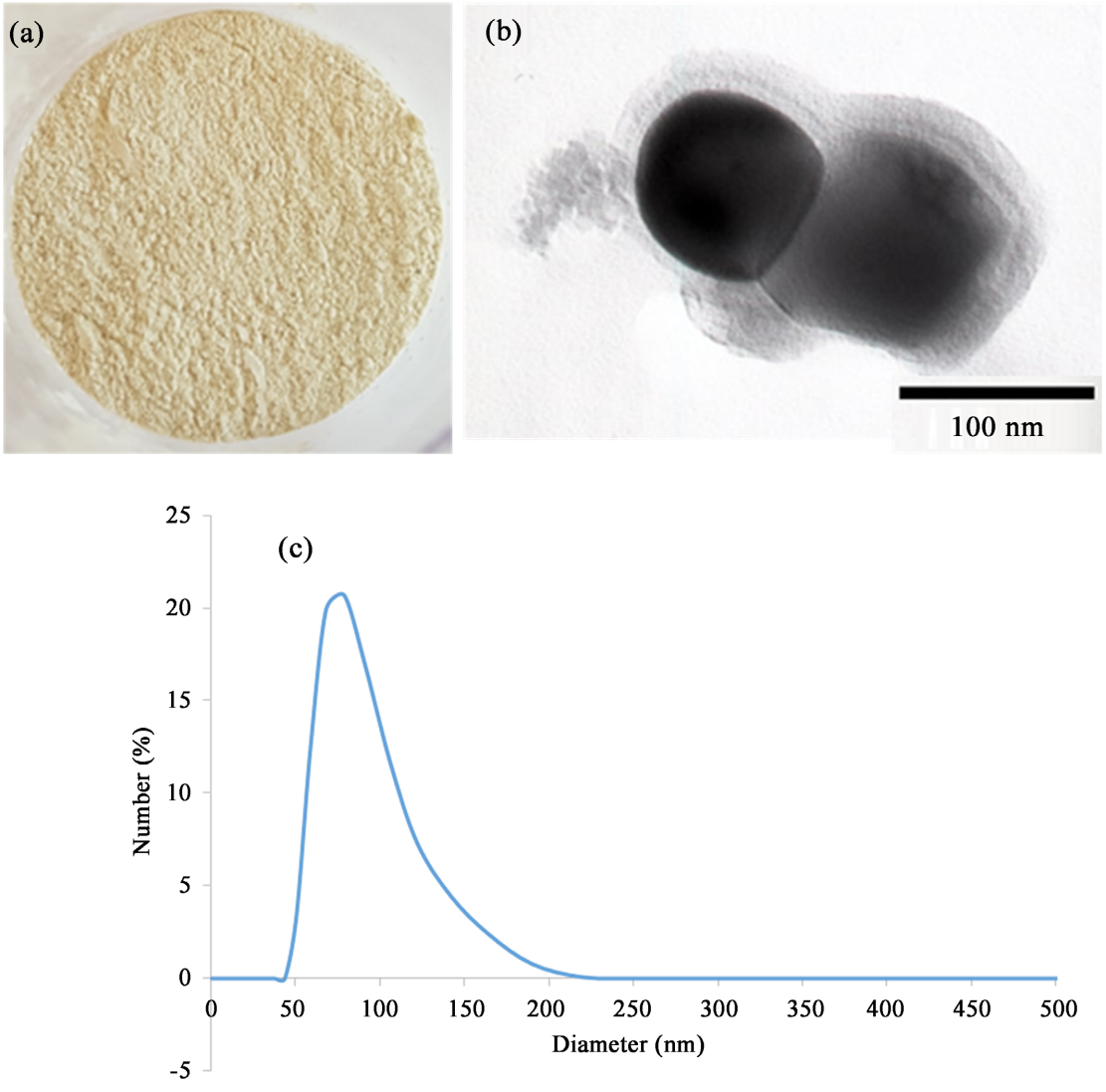


Figure 2. (a) Ferroelectric inorganic perovskite nanopowder from PZN-4.5PT, (b) TEM images showing spherical shapes (c) Size distribution of PZN-4.5PT nanoparticles.

The presence of a blackish coloration on certain areas of the surface may be due to the sensitizer (EB-PeryDA) or the organic matrix (CC) containing the nanoparticles. This image shows compact nano-composite on the surface revealing the presence of an organic compound serving as a binder between the nanoparticles grains which appear to be coalesced. It suggests that the EB-PeryDA causes coalescence of grains by diffusion through the pores. The morphology of the surface is initially linked to the energy of the particles and the organic matrix.

The SEM image in Figure 3(b) confirms the clear difference in morphology between the theoretically superimposed layers as shown in Figure 3(c) (Glass/ITO/$TiO_2$/np-CC/EB-PeryDA/Ag). The perovskite nanoparticle layer is well embedded in the $TiO_2$ forming a $TiO_2$/np-CC/EB-PeryDA nano-composite with thicknesses up to 400 nm for the np-CC layer and up to 312 nm for that of EB-PeryDA (Figure 3(b)). This good crystallization and the lack of enormous porosity significantly reduce the recombination of non-radiative charge carriers, which is likely to occur at entrapment sites associated with grain boundaries. The different layers with their activation energy have been shown to explain the role of each. Thus, the activation energy (1.67 eV) of the perovskite layer corresponds

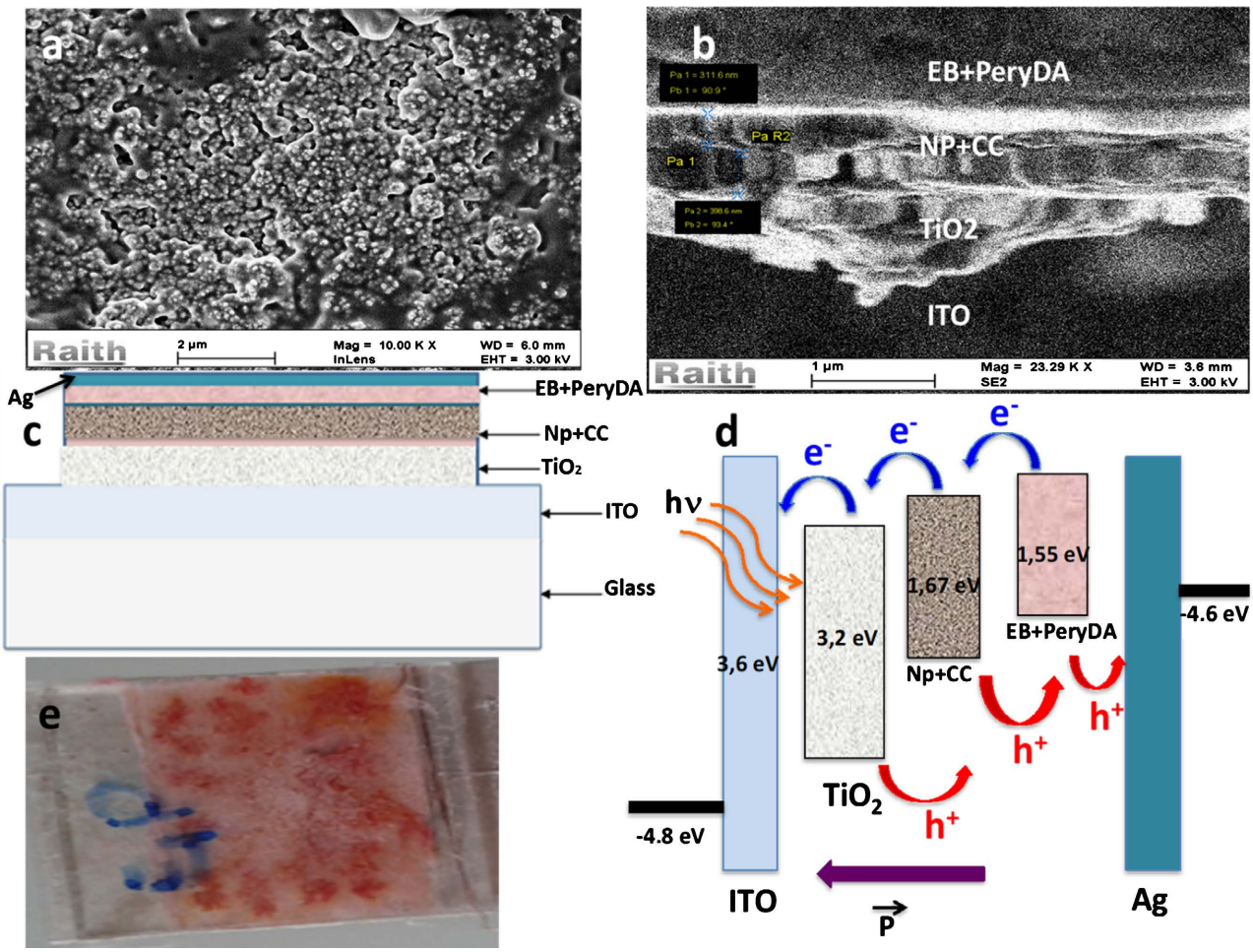


Figure 3. SEM images (a) in top view, (b) in transverse view, (c) illustration in transverse mode of the different layers deposited on ITO substrate, (d) diagram of the energy bands of the different layers and (e) photo of a fabricated Ferro-OPV solar cell.

perfectly with the values often obtained for the best absorbent layers. For the EB layer on Perylene Diimide Aniline (EB-PeryDA), it consists mainly of a molecule derived from perylene which is an acceptor molecule which can also act a sensitizing role (absorption) thanks to its energy rather weak activation of 1.55 eV. Figure 3(d) shows the diagram of the energy bands of the different layers. Finally, Figure 3(e) is a photo of one of the different Ferro-OPV solar cells produced and which allowed us to perform different tests and characterizations.

### 4.2. Optical Characterization

Figure 4 shows the UV-Visible reflectance, transmittance and absorbance spectra of the ITO reference substrate (Figure 4(a)), PZN-4.5PT nanoparticles absorbance (Figure 4(b)), ITO/$TiO_2$/np-CC layer reflectance, transmittance and absorbance (Figure 4(c)), transmittance and absorbance spectra of the Ferro-OPV cell (Figure 4(d)).

Absorption peak from the PZN-4.5PT nanoparticles is located at 213 nm. For the ITO reference sample composed by an ITO layer only on a glass substrate, there is an increase of the transmission more than 80% in the entire visible and near infrared spectral band, while the absorption and reflection percentage is quite low in this range. On the other hand, this transmission decreases with the deposition of the ITO/$TiO_2$/np-CC layers, ITO/$TiO_2$/np-CC/PeryDA and ITO/$TiO_2$/np-CC/EB-PeryDA respectively (Figure 4(d)). We also see a remarkable

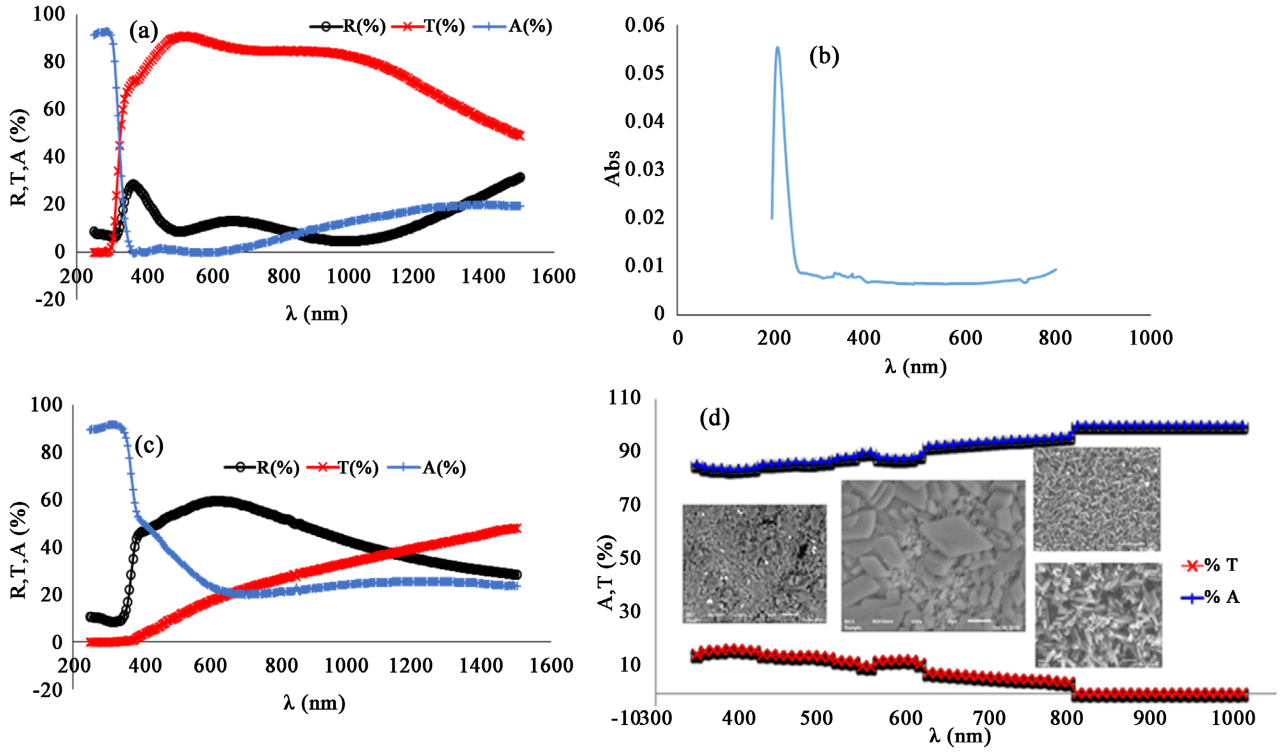


Figure 4. (a) UV-Visible reflectance (R), transmittance (T) and absorbance (A) spectra of the ITO as a reference, (b) PZN-4.5PT nanoparticles absorbance, (c) R, T and A of ITO/$TiO_2$/np-CC thin film, (d) transmittance and absorbance spectra of the Ferro-OPV fabricated solar cell.

effect of the third sensitizing layer (EB-PeryDA), namely the considerable increase in absorption and its spreading throughout the visible and near infrared range. This increase in absorption was limited in the visible range up to about 600 nm (Figure 4(c)). It should also be noted that the effect of these layers is, above all, to reduce the optical gap which is located at approximately 1.66 eV for the layer of ferroelectric perovskite nanoparticles in the biopolymer.

Figure 5 shows the PL spectra of the PZN-4.5PT nanoparticles excited at 205 nm, ITO/$TiO_2$/np-CC thin film and ITO/$TiO_2$/np-CC/EB-PeryDA sample measured by excitation at $\lambda$ex = 330 nm. According to Figure 5(a) the PZN-4.5PT nanoparticles covered the PL range of 300 - 600 nm with very weak intensity. Using this property, ITO/$TiO_2$/np-CC thin film PL intensity was improved in the same range from 800 to around 3,000,000 counts/s (Figure 5(b)). One can observe the presence of different emission peaks probably coming from the various organic molecules in the CC biopolymer. The fabricated solar cell PL spectrum is the sum of these different layers emissions permitting to achieve full coverage in the visible range of the spectrum (Figure 5(c)). Color coordinates

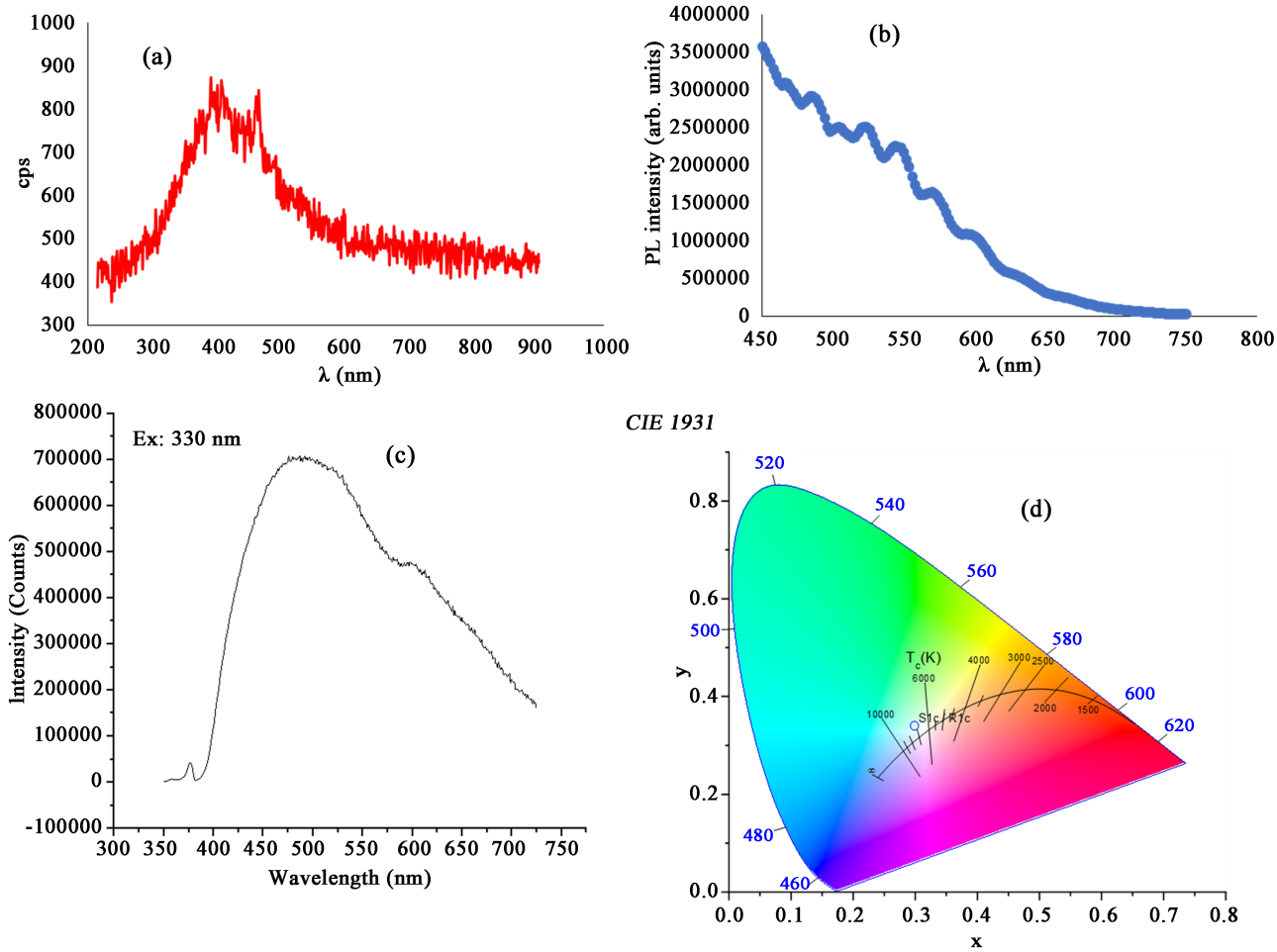


Figure 5. PL spectra of (a) PZN-4.5PT nanoparticles, (b) PZN-4.5PT nanoparticles dispersed in the biopolymer matrix thin film (ITO/$TiO_2$/np-CC), (c) ITO/$TiO_2$/np-CC/EB-PeryDA thin film and (d) CIE-1931 chromaticity diagram of ITO/$TiO_2$/np-CC/EB-PeryDA thin film.

are one of the important factors to evaluate the luminescence materials performance. For our sample the color coordinates are represented in the CIE (Commission Internationale de l'Eclairage) chromaticity diagram as shown in **Figure 5(d)**. The color coordinates (x = 0.30, y = 0.34) is close to the ideal reference white light source CIE coordinates (x = 0.33, y = 0.33). This result suggests that this material is very interesting for single material white light source applications.

### 4.3. Electrical Characterization

The architecture of the device used in this study is given in **Figure 3(c)** and **Figure 3(d)**. The as fabricated cell gave an exceptional record efficiency of 39.32% with an open voltage circuit ( $V_{oc}$) of 3.50 V, a short-circuit current density ($J_{sc}$) of 0.118 mA/cm$^2$ and an FF of 0.72 with an incident power of 3825 lux (5.6 W/m$^2$) measured in positive direction (**Figure 6(a)**). The power - voltage dependence curve of this cell is illustrated in **Figure 6(b)**. A maximum power of 220 μW/cm$^2$ is obtained. This is explained by the low short-circuit current density. However, this value is large compared to the majority of generated power from indoor solar cells in literature which record is 301.6 μW/cm$^2$ [28]. For the J-V

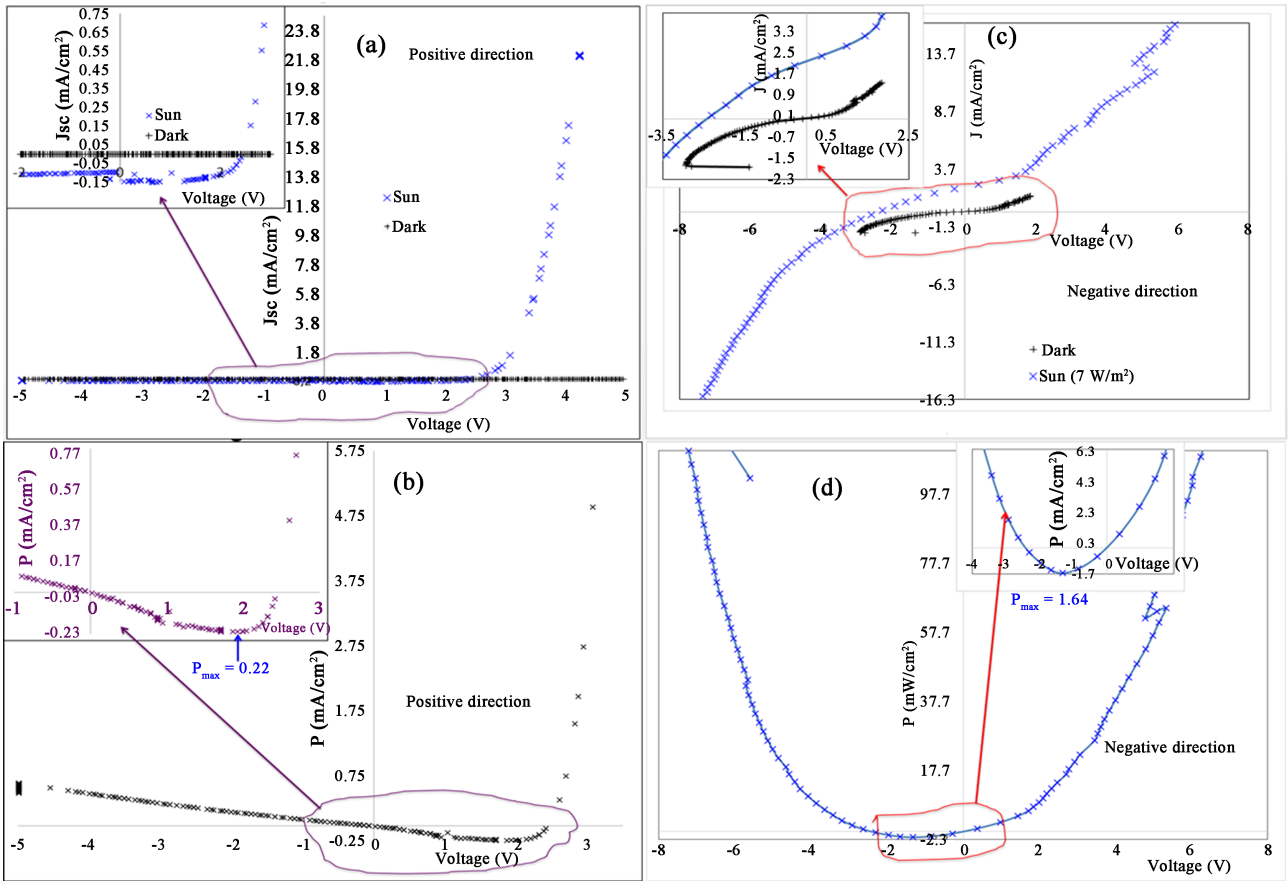


**Figure 6.** Characteristics (a) current - voltage (J-V) and (b) power - voltage (P-V) of the Ferro-OPV solar cell under dark and under an incident lightning of 5.6 W/m$^2$ in the direction of polarization of the ferroelectric layer (+ on ITO), (c) current - voltage (J-V) and (d) power - voltage (P-V) of the Ferro-OPV solar cell under dark and under lightning of 7 W/m$^2$ in the opposite direction to the direction of the polarization of the ferroelectric layer (+ on Ag).

measurement in negative direction with a power of 4781 lux (7 W/m²), we obtained a current density of 2 mA/cm², an open circuit voltage of 2.30 V and a fill factor of 0.35. The behavior of this J-V curve is typical of ferrophotovoltaic materials which have a characteristic of being either in the quadrant (V > 0 and J < 0) for the direction opposite to the direction of polarization, or in quadrant (V < 0 and J > 0) in the same direction. This is what we observe in **Figure 6(c)** and **Figure 6(d)**. We notice that the current density is higher than that obtained in the first case (2 mA/cm² instead of 0.118 mA/cm²) with a small open circuit voltage $V_{oc}$ of 2.30 V instead 3.5 V for the first one. The interesting result is the improving of the power delivered by the device from 220 μW/cm² to a record of 1700 μW/cm² for indoor application solar cells knowing the record is 301.6 μW/cm² as published in [28] in 2021. These high values of $V_{oc}$ and generated power would open large potential application for many electronic devices empowering.

For investigation on the effects of different components and layers of the solar cells we realized I-V characteristics of different solar cells composed by ITO/$TiO_2$/np-CC (**Figure 7**, blue star curve), ITO/$TiO_2$/np-CC/EB **Figure 7**, black x curve), ITO/$TiO_2$/np-CC/PeryDA (**Figure 7**, purple triangle curve) and ITO/$TiO_2$/np-CC/EB-PeryDA (**Figure 7**, red +) under 4781 lux incident light. From this figure, the values of $V_{oc}$, $J_{sc}$ and FF were 2V, 0.032 mA/cm² and 0.20 respectively for the PZN-4.5PT nanoparticles in CC solar cell. The value of $V_{oc}$ decreased from 2 to 0.19 V and the short current density from 0.032 to 0.001 mA/cm², showing that the high value of $V_{oc}$ is coming from the ferroelectric

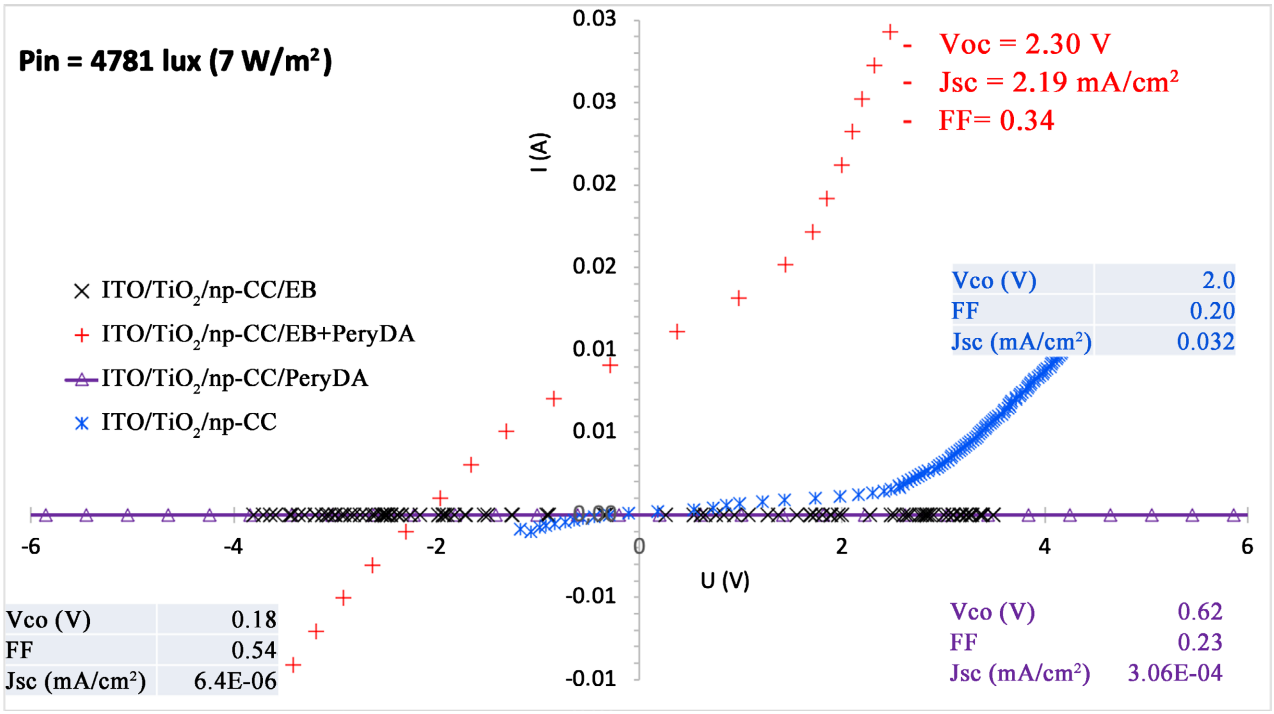


**Figure 7.** I-V characteristics of different solar cells composed by (blue star) ITO/$TiO_2$/np-CC, (black x) ITO/$TiO_2$/np-CC/EB, (purple triangle) ITO/$TiO_2$/np-CC/PeryDA and (red +) ITO/$TiO_2$/np-CC/EB-PeryDA.

nanoparticles presence in the device. In the other hand the fall down of the $J_{sc}$ value revealed that the EB is like more insulating material than conductive one and can inhibit the ferroelectric effect. Adding a PeryDA on the nanoparticles in CC layer, the $V_{oc}$ increased from 0.18 to 0.60 V while the $J_{sc}$ remains very low. This means that the excellent values from the cell are not from the PeryDA only also. The combination of these different components in the detailed architecture permitted to reach very high values for $V_{oc}$ of 2.30 V, for $J_{sc}$ of 2.19 mA/cm$^2$ and a FF of 0.34. These results indicate that the presence of any of these different materials layers is fundamental to get such important electrical characteristics.

To understand the time stability of the fabricated solar cell, we studied the variation of $V_{oc}$ and $J_{sc}$ for different values of the incident power (**Figure 8(a)** and **Figure 8(b)**). $V_{oc}$ shows increasing with light intensity and remains time independent till 28 min exposure. However, for the incident light of 105 w/m$^2$, the $V_{oc}$ value decreased in this range and suddenly increased exponentially to more than 20 V over 28 min. Thus, the maximum voltage is reached and does not change anymore. The only possible explanation is that exposure to a given light intensity creates photoelectrons which are transported to the $TiO_2$/np-CC and/or np-CC/EB-PeryDA interfaces. The presence of the ferroelectric layer between these interfaces will facilitate the accumulation of charges towards these interfaces. Indeed, a recent study showed us that these ferroelectric layers have capacities or polarization which depends on the luminosity [29]. Longer the exposure time increases, more excitons are created and the more the charge accumulation

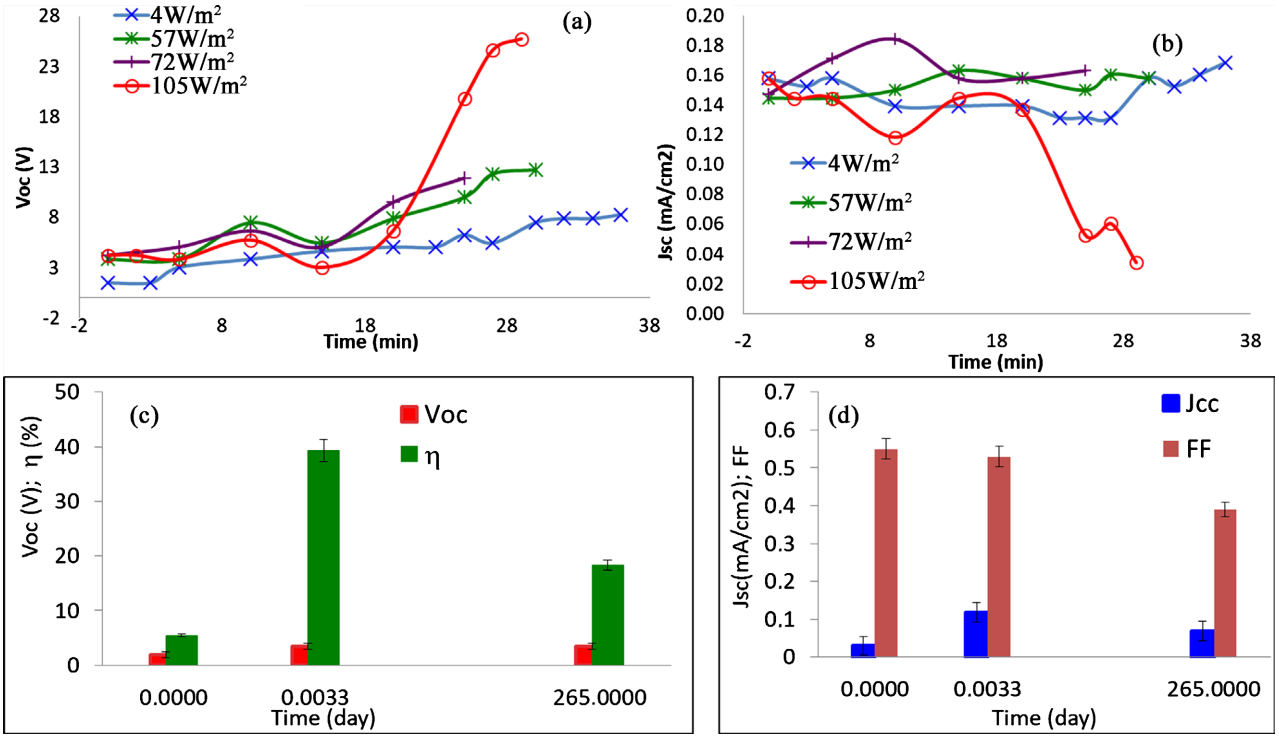


**Figure 8.** (a) Stability in time of the open-circuit voltage $V_{oc}$ of (b) the short-circuit current $J_{sc}$ under different light powers continuously for about thirty minutes and comparison of the photovoltaic characteristics: (c) $V_{oc}$ and FF, (d) $J_{sc}$ and $\eta$ between a freshly manufactured cell and the same cell one year later under an incident power of 5.6 W/m$^2$.

increases to reach a plateau. The photocurrent is dependent on the illumination intensity as shown in Figure 8(b) with a slight decrease as the irradiance increases. On the other hand, at the same time, a long exposure under high lighting (over 105 W/m$^2$) makes it possible the creation and increasing of photogenerated activated defects, thus increasing the recombination rate at the ITO/$TiO_2$ and EB-PeryDA/Ag interfaces. This will result in a significant reduction in the current density that can flow. This theory seems to be the best explanation and is supported by the fact that increasing light intensity decreases short-circuit current density.

Thus, the large increase in $V_{oc}$, with light intensity increasing, compensates the $J_{sc}$ decreasing, so the efficiency remains very high at low lighting. So, with a fairly high lighting (>105 W/m$^2$), the recombination rate becomes too high and drastically reduce the $J_{sc}$, which leads to a low efficiency compared to that of 4 W/m$^2$.

The same solar cell that obtained an efficiency of 39.32% was characterized one year after production to see the stability over time of these cells. Thus in Figure 8(c) and Figure 8(d), the maximum efficiency of 39.32% has decreased by about 53% to be at 18.37% as indicated in Table 1. At the same time $V_{oc}$ practically remains unchanged while $J_{sc}$ has fallen from 0.118 mA/cm$^2$ to 0.069 mA/cm$^2$ as the FF which went from 0.72 to 0.39. These results support the above explanation of the effect of illumination on the characteristics of the solar cell, which is closely linked to the presence of the ferroelectric perovskite layer.

As shown in Figure 6(a) and Figure 6(c) the biomaterials (CC and EB) and sensitizers (EB-PeryDA) significantly improved the performance, particularly the efficiency and $V_{oc}$ of the device compared to perovskite solar cells. The average efficiency for nine measurements carried out was 39.32% with a short-circuit current density ($J_{sc}$) of 0.118 mA/cm$^2$ for the sample measured in the positive direction, an open circuit voltage ( $V_{oc}$) of 3.5 V and a fill factor (FF) of 0.72. The substantial performance improvement produced by our device is reflected in the values of all halogenated perovskite photovoltaic cells. The best efficiency produced by indoor application solar cells is around 40.1% in 2021 [28]. However, it is expected with our optimized solar cell to find more than 50% efficiency under low incident light.

## 5. Conclusions

This simple but effective method is developed to improve the cell performance

Table 1. Photovoltaic parameters of the Ferro-OPV solar cell.

| Time | Direction of circuit connection | $V_{oc}$ (V) | $J_{sc}$ (mA/cm$^2$) | FF | Pin (W/m$^2$) | Pmax (mW/cm$^2$) | $\eta$ (%) | $\Delta\eta$ |
|---|---|---|---|---|---|---|---|---|
| 0 | Direction + | 3.5 | 0.118 | 0.72 | 5.6 | 0.22 | 39.32 | |
| 265 days after | Direction + | 3.43 | 0.069 | 0.39 | 5.6 | 0.092 | 18.37 | −53.28 |
| [28] | - | 1 | 0.152 | 0.79 | - | - | 40.1 | - |
| [30] | - | 1.1 | 0.09 | 0.79 | - | - | 26.1 | - |

via the combination of ferroelectric perovskite nanoparticles dispersed in a biopolymer matrix and different conducting layer molecule. We, successfully, fabricated a ferroelectric PZN-4.5PT nanoparticles thin film using a biopolymer as matrix. More than 4 $cm^2$ hybrid ferro-OPV solar cell, using low cost technique with very high efficiency ($\eta$ = 39.2%) and a record $V_{oc}$ of 3.5 V for indoor application, was performed. A record of 1.64 $mW/cm^2$ generated power was reached under 4781 lux (7 $W/m^2$) boosting the possible application of this type of solar cell for low power devices energy autonomy.

Long exposure under high lighting (over 105 $W/m^2$) makes it possible the creation and increasing of photogenerated activated defects, thus increasing the recombination rate at the ITO/$TiO_2$ and EB-PeryDA/Ag interfaces.

The low perovskite nanoparticles and the Organic Biopolymer used as matrix and conducting layer molecule make this device one of the best friendly environmental perovskite solar cells.

## Acknowledgements

This work is supported by Agence Universitaire de la Francophonie (AUF).

## Conflicts of Interest

The authors declare no conflicts of interest regarding the publication of this paper.

## References

[1] Etgar, L., *et al.* (2012) *Journal of the American Chemical Society*, **134**, 17396-17399. https://doi.org/10.1021/ja307789s

[2] Noh, J.H., Im, S.H., Heo, J.H., Mandal, T.N. and Seok, S.I. (2013) *Nano Letters*, **13**, 1764-1769. https://doi.org/10.1021/nl400349b

[3] Wang, K., *et al.* (2019) *Advanced Materials*, **31**, Article ID: 1902037. https://doi.org/10.1002/adma.201902037

[4] Wang, D., Wright, M., Elumalai, N.K. and Uddin, A. (2016) *Solar Energy Materials and Solar Cells*, **147**, 255-275. https://doi.org/10.1016/j.solmat.2015.12.025

[5] Jawher, R., Chtourou, R., Sallet, V. and Oueslati, M. (2023) *Materials Science and Engineering*: *B*, **287**, Article ID: 116146. https://doi.org/10.1016/j.mseb.2022.116143

[6] Akhavan, O., Tohidi, H. and Moshfegh, A.Z. (2009) *Thin Solid Films*, **517**, 6700-6706. https://doi.org/10.1016/j.tsf.2009.05.016

[7] Grinberg, I., *et al.* (2013) *Nature*, **503**, 509-512. https://doi.org/10.1038/nature12622

[8] Ndioukane, R., *et al.* (2019) *EPL*, **125**, 47004. https://doi.org/10.1209/0295-5075/125/47004

[9] Atzori, L., Iera, A. and Morabito, G. (2010) *Computer Networks*, **54**, 2787-2805. https://doi.org/10.1016/j.comnet.2010.05.010

[10] Gubbi, J., Buyya, R., Marusic, S. and Palaniswami, M. (2013) *Future Generation Computer Systems*, **29**, 1645-1660. https://doi.org/10.1016/j.future.2013.01.010

[11] Al-Fuqaha, A., Guizani, M., Mohammadi, M., Aledhari, M. and Ayyash, M. (2015) *IEEE Communications Surveys & Tutorials*, **17**, 2347-2376.

https://doi.org/10.1109/COMST.2015.2444095

[12] Khan, J.A., Qureshi, H.K. and Iqbal, A. (2015) *Computers and Electrical Engineering*, **41**, 159-176. https://doi.org/10.1016/j.compeleceng.2014.06.009

[13] Yin, H., *et al.* (2018) *Journal of Materials Chemistry A*, **6**, 8579-8585. https://doi.org/10.1039/C8TA01728J

[14] Lee, H.K.H., Li, Z., Durrant, J.R. and Tsoi, W.C. (2016) *Applied Physics Letters*, **108**, Article ID: 253301. https://doi.org/10.1063/1.4954268

[15] Minnaert, B. and Veelaert, P. (2014) *Energies*, **7**, 1500-1516. https://doi.org/10.3390/en7031500

[16] Freitag, M., *et al.* (2017) *Nature Photonics*, **11**, 372-378. https://doi.org/10.1038/nphoton.2017.60

[17] Teran, A.S., *et al.* (2016) *IEEE Transactions on Electron Devices*, **63**, 2820-2825. https://doi.org/10.1109/TED.2016.2569079

[18] Li, B., Hou, B. and Amaratunga, G.A.J. (2021) *InfoMat*, **3**, 445-459. https://doi.org/10.1002/inf2.12180

[19] Mori, S., *et al.* (2015) *Japanese Journal of Applied Physics*, **54**, Article ID: 071602. https://doi.org/10.7567/JJAP.54.071602

[20] De Rossi, F., Pontecorvo, T. and Brown, T.M. (2015) *Applied Energy*, **156**, 413-422. https://doi.org/10.1016/j.apenergy.2015.07.031

[21] Cutting, C.L., Bag, M. and Venkataraman, D. (2016) *Journal of Materials Chemistry C*, **4**, 10367-10370. https://doi.org/10.1039/C6TC03344J

[22] Cao, Y., Liu, Y., Zakeeruddin, S.M., Hagfeldt, A. and Grätzel, M. (2018) *Joule*, **2**, 1108-1117. https://doi.org/10.1016/j.joule.2018.03.017

[23] Li, M., *et al.* (2018) *Advanced Energy Materials*, **8**, Article ID: 1801509. https://doi.org/10.1002/aenm.201801509

[24] Lee, H.K.H., *et al.* (2018) *Journal of Materials Chemistry A*, **6**, 5618-5626. https://doi.org/10.1039/C7TA10875C

[25] Liu, X., Huettner, S., Rong, Z., Sommer, M. and Friend, R.H. (2012) *Advanced Materials*, **24**, 669-674. https://doi.org/10.1002/adma.201103097

[26] Lin, Y. and Zhan, X. (2014) *Materials Horizons*, **1**, 470-488. https://doi.org/10.1039/C4MH00042K

[27] Ndioukane, R., Kobor, D., Solard, J. and Motte, L. (2019) *OAJ Materials and Devices*, **4**, 1502. https://doi.org/10.23647/ca.md20191502

[28] He, X., *et al.* (2021) *Advanced Materials*, **33**, Article ID: 2100770. https://doi.org/10.1002/adma.202100770

[29] Quattropani, A. (2018) Synthesis of Ferroelectric Oxides for Photovoltaic Applications. PhD Thesis, Strasbourg University, Strasbourg.

[30] Cui, Y., *et al.* (2019) *Nature Energy*, **4**, 768-775. https://doi.org/10.1038/s41560-019-0448-5